View metadata, citation and similar papers at core.ac.uk

brought to you by CORE

provided by NASA Technical Reports Server

HYDRAULIC FORCES ON A CENTRIFUGAL IMPELLER UNDERGOING SYNCHRONOUS WHIRL*

Paul E. Allaire
University of Virginia
Charlottesville, Virginia 22901

Cheryl J. Sato
BE&K Engineering Company
Birmingham, Alabama 35243

Lyle A. Branagan
Pacific Gas and Electric Company
San Ramon, California 94583

High speed centrifugal rotating machinery can have large vibrations caused by aerodynamic forces on impellers. This work develops a method of calculating forces in a two dimensional orbitting impeller in an unbounded fluid with non-uniform entering flow. A finite element model of the full impeller is employed to solve the inviscid flow equations. Five forces acting on the impeller are included: Coriolis forces, centripetal forces, changes in linear momentum, changes in pressure due to rotation and pressure changes due to linear momentum. Both principal and cross-coupled stiffness coefficients are calculated for the impeller. Agreement with experimental results is fair.

NOMENCLATURE

A_3	Impeller discharge area, $A_3 = 2\pi R_{3b}$
b	Impeller thickness
F	Force
F_{xx}	Principal force
F_{yx}	Cross-coupling force
K	Stiffness
K_{xx}	Principal stiffness
K_{yx}	Cross-coupled stiffness
$\overline{K}_{xx}$	Dimensionless principal stiffness
$\overline{K}_{yx}$	Dimensionless cross-coupled stiffness
P	Pressure
Q	Flow rate
r	radius
R_1	Inner radius of inner flow region
R_2	Inner radius of impeller
R_3	Outer radius of impeller
R_4	Outer radius of outer flow region
U_3	Impeller tip speed, $U_3 = \Omega R_3$
$\vec{V}$	Particle velocity in reference frame
Δx	Displacement in positive x-direction
Δy	Displacement in positive y-direction

*This work was funded in part by NASA Contract NAG 3-180.

β	Blade angle
Γ	Circulation
ε	Eccentricity
θ	Angle with respect to the x-axis
θ_c	Unknown angle approximated by the blade sweep angle
θ_s	Blade sweep angle
ρ	Density of fluid
ϕ	Velocity potential
ψ	Stream function
$\overline{\psi}$	Dimensionless stream function
Ω	Rotor rotation speed

INTRODUCTION

Vibration problems in turbomachinery such as the U.S. Space Shuttle turbopumps (ref. 1) are an important issue in industry. Considerable efforts have been made to understand their causes and prevent catastrophic failure. Modifications in the bearings, dampers and seals (ref. 1,2) in a given machine can often alleviate such problems, but are not always effective. Because relatively little is known about the influence of an impeller on vibrations, it is of interest to investigate impeller force levels in attempts to further understand and reduce vibration problems.

It is known that fluid forces act on an impeller during operation and often initiate serious vibration problems, but they are not easy to calculate. Initially, the impeller may be displaced due to residual unbalances or other causes. Impeller forces then arise both parallel to and perpendicular to the direction of displacement. They are known as hydraulic or aerodynamic forces. This phenomenon can be additive, such that a small perturbation can eventually result in large vibrations and possible shaft failure. Several works concerning rotor dynamics and flow in impellers have been published, but relatively few papers have dealt with the calculation of aerodynamic forces on impellers.

A study of aerodynamic forces on centrifugal impellers, published by Colding-Jorgensen (ref. 3), involved calculating the impeller force caused by rotor eccentricity along with the associated stiffness and damping coefficients. The final objective was to determine the effect of this force on rotor stability. Two-dimensional potential flow was used, representing the impeller by a source-vortex point. The diffuser was modelled by a distribution of vortices and the flow field was solved by the singularity method. The velocity induced by the singularity distribution on the diffuser was considered to be a parallel stream; thus, the impeller force was obtained by relating the impeller to a body with circulation, influenced by a source, and in a parallel stream, and using the theorems of Joukowski and Lagally.

Shoji and Ohashi (ref. 4) calculated fluid forces on a centrifugal impeller using unsteady potential theory. Incompressible, two-dimensional flow was assumed and the rotating axis whirled at constant speed. Other assumptions included shockless entry at the leading edges of the blades and the Kutta condition at the trailing edges. Free vortices were assumed to be shed from the trailing edges and carried downstream with steady velocities along steady streamlines, and blade thickness was neglected. The forces acting on the impeller were calculated by integrating the pressure distribution on the blades.

Recently, Imaichi, Tsujimoto and Yoshida (ref. 5) analyzed unsteady torque on a two-dimensional radial impeller using singularity methods. They recognized that studies of unsteady flow were necessary for prediction of unsteady forces on an impeller but unsteady torque was examined because it was one of the most typical unsteady characteristics of impellers. It was shown that unsteady torque could be divided into three components: quasisteady, apparent mass, and wake. The wake component was usually found to be the smallest quantity. Approximations of fluctuating torque were made using apparent mass coefficients for various blade angles, blade numbers and diameter ratios of logarithmic impellers.

Iino's work (ref. 6) dealt with potential interaction between a centrifugal impeller and a vaned diffuser. The dynamic load on the impeller blades due to this interaction was examined. Unsteady flow was analyzed using the method of singularities assuming two-dimensional, potential flow and infinitely thin blades. The unsteady Bernoulli equation for a rotating coordinate system was used to solve for the unsteady pressures. Pressure distributions were examined for various impeller configurations. Load distribution on diffuser blades was related to pressure fluctuations; the dynamic load on impeller blades was affected by consideration of this load distribution.

An unbounded eccentric centrifugal impeller with an infinite number of logarithmic spiral blades was considered by Allaire et al. (ref. 7). A simple kinematic analysis of flow in the impeller was carried out and impeller stiffnesses calculated. Fire forces acting on the eccentric impeller were identified: Coriolis forces, centripetal forces, changes in linear momentum, changes in pressure due to rotation and pressure changes due to linear momentum.

In addition to theoretical studies of forces on impellers, some work has been done experimentally. A paper on experimental measurement was presented by Uchida, Imaichi and Shirai (ref. 8). They measured radial forces on a centrifugal pump with a volute and examined the effect of the cross-sectional area and shape of the volute tongue on the force. The dynamic component of force and the effect of cavitation on the force were also investigated.

Research by Kanki, Kawata and Kawatani (ref. 9) also involved experimentally measuring forces on a centrifugal pump impeller. They specifically measured hydraulic radial forces on impellers with double volutes or vaned diffusers. Both static and dynamic loads were measured with varying flow rates.

Chamieh et al. (ref. 10) measured hydrodynamic stiffnesses experimentally for a centrifugal pump impeller with a volute. Forces on the impeller were measured as the center of rotation was orbited for low frequencies. Pressure distributions around the volute were obtained and static pressure forces were measured, providing a more complete force analysis.

This paper examines centrifugal impellers and develops a method of calculating the forces induced by eccentric operation. The analysis is done in a rotating reference frame and considers a two-dimensional, unbounded impeller with synchronous motion. Incompressible, potential flow is assumed. The analysis utilizes the finite element method to solve for the flow field. A control volume formulation is used to calculate the forces acting on the shaft of an eccentric impeller. Stiffnesses are computed for different impeller designs. Plots of the finite element meshes as well as corresponding streamline plots are included, along with velocity profiles and graphs of stiffnesses versus blade number and blade angle.

METHOD OF ANALYSIS

The two dimensional impeller region is divided into three regions: inlet region, blade region, and outlet region. Figure 1 shows the three regions with one blade for illustration purposes. Potential flow is assumed in the analysis with the radial flow calculated using a velocity potential and the tangential flow calculated using a stream function (ref. 11,12). Both ϕ and ψ satisfy Laplace's equation

$$\nabla^2\phi = 0 \tag{1}$$

$$\nabla^2\psi = 0 \tag{2}$$

in the region between R_1 and R_4.

Two cases are considered - impeller centered and impeller eccentric. In the first case, the impeller blades are centered in the coordinate system. The flow through each blade passage is the same. For the second case, the inlet flow is assumed centered at the origin while the impeller is physically moved the distance ε along the x axis (in the relative coordinate system). Thus the flow through the passages on the positive x axis side is smaller than the flow through those on the negative x axis side. A typical value of $\varepsilon_1/R_2 = 0.0025$ was used. It was found that varying ε_1/R_2 from 0.01 to 0.00125 changed the calculated stiffness by less than 10%.

For the radial flow, the boundary condition at the inlet is that due to a source at the origin

$$\left.\frac{\partial\phi}{\partial n}\right|_{r=R_1} = \frac{Q}{2\pi R_1 b} \tag{3}$$

and no flow is allowed through the blades

$$\left.\frac{\partial\phi}{\partial n}\right|_{\text{Blade}} = 0 \tag{4}$$

If the shaft is centered, the outlet boundary condition is

$$\left.\frac{\partial\phi}{\partial n}\right|_{r=R_4} = \frac{Q}{2\pi R_4 b} \tag{5}$$

In the case of an eccentric shaft, the exit flow cannot be uniform around the impeller. It is assumed to depend upon the angle θ with the form (ref. 13)

$$\left.\frac{\partial\phi}{\partial n}\right|_{r=R_4} = \frac{Q}{2\rho R_4 b}\left[1 - \frac{\varepsilon_4}{R_4}\right]\cos(\theta-\theta_c) \tag{6}$$

where θ_c is the approximate sweep angle. It was found that varying the sweep angle by $\pm$ 10 degrees changed the stiffnesses by approximately 1% or less.

With tangential flow, the boundary conditions at the inner and outer radii are

$$\psi|_{r=R_1} = -\frac{\Gamma}{2\pi}\ln R_1$$

$$\psi|_{r=R_4} = -\frac{\Gamma}{2\pi}\ln R_4$$

However, for vortex flow representing an impeller with angular velocity Ω, the value for Γ is

$$\Gamma = -2\pi \Omega R_2^2$$

The boundary conditions become

$$\psi|_{r=R_1} = \Omega R_2^2 \ln R_1 \tag{7}$$

$$\psi|_{r=R_4} = \Omega R_2^2 \ln R_4 \tag{8}$$

Along the blade, the stream function is an unknown constant.

$$\psi|_{\text{Blade}} = \text{Constant} \tag{9}$$

The constant is evaluated when the total flow, due to the superposition of radial and tangential flow, satisfies the Kutta condition at the trailing edge of all blades. A Newton-Raphson iteration process is used to obtain values of stream function on the blades. In the centered case, the stream function over all of the blades is the same while it varies for the eccentric case.

Finite elements (ref. 14,15) were used to solve Laplace's equation for both the radial and tangential flow. A typical mesh is shown in Figure 2. Because of the large number of nodes, a profile solver (ref. 14) was required. Finite width blades were included in the analysis.

FORCES AND STIFFNESS

The net surface force on the control volume (analysis region) is (ref. 16)

$$\vec{F}_s = \int_{CV} \left[2\vec{\Omega} \times \vec{V} + \vec{\Omega} \times (\vec{\Omega} \times \vec{r}) \right] \rho \, d\forall + \int_{CS} \vec{V} \; \rho \vec{V} \cdot d\vec{A} \tag{10}$$

The surface forces are composed of the pressure forces on the control volume ($\vec{F}_p$) and the forces of the shaft on the control volume ($\vec{F}_{SHAFT}$). Thus,

$$\vec{F}_s = \vec{F}_{SHAFT} + \vec{F}_p$$

From the Bernoulli equation for a rotating reference frame:

$$\frac{P}{\rho} - \frac{1}{2} |\vec{\Omega} \times \vec{r}|^2 + \frac{1}{2} |\vec{V}|^2 = \text{constant} \tag{11}$$

This can be solved for pressure and integrated over the control surface:

$$\int_{CS} P \, dA = \int_{CS} \left\{ \frac{\rho}{2} \left[|\vec{\Omega} \times \vec{r}|^2 - |\vec{V}|^2 \right] + \text{constant} \right\} d\vec{A} \tag{12}$$

The forces due to pressure are expressed as:

$$\vec{F}_p = -\int P \, d\vec{A} \tag{13}$$

since the force vector is opposite the area vector.

The force on the shaft due to control volume is

$$\begin{aligned}
\vec{F}_{\substack{ON \\ SHAFT}} &= -\vec{F}_{SHAFT} = \vec{F}_p - \vec{F}_s \\
\vec{F}_{\substack{ON \\ SHAFT}} &= -\int_{cs} \frac{\rho}{2} \left[|\vec{\Omega} \times \vec{r}|^2 - |\vec{V}|^2 \right] d\vec{A} \\
&\quad - \int_{cv} \left[2\vec{\Omega} \times \vec{V} + \vec{\Omega} \times (\vec{\Omega} \times \vec{r}) \right] \rho d\forall \\
&\quad - \int_{cs} \vec{V} \; \rho \vec{V} \cdot d\vec{A}
\end{aligned} \tag{14}$$

The five components of this force are:

1. $-\int_{cv} \rho (2 \vec{\Omega} \times \vec{V}) \, d\forall$ — Coriolis force

2. $-\int_{cv} \rho \, \vec{\Omega} \times (\vec{\Omega} \times \vec{r}) \, d\forall$ — Centripetal force

3. $-\int_{cs} \vec{V} \; \rho \vec{V} \cdot d\vec{A}$ — Force due to change in linear momentum

4. $-\int_{cs} \frac{\rho}{2} |\vec{\Omega} \times \vec{r}|^2 \, d\vec{A}$ — Force due to change in pressure due to rotation

5. $\int_{cs} \frac{\rho}{2} |\vec{V}|^2 \, d\vec{A}$ — Force due to change in pressure due to change in linear momentum

For the finite element analysis, the integral expressions are used in summation form.

Stiffness is defined as the negative of the change in force divided by the change in displacement, or:

$$K = -\frac{\Delta F}{\Delta x}$$

In this analysis, principal (K_{xx}) and cross-coupled (K_{yx}) stiffnesses are calculated, where:

$$K_{xx} = -\frac{\Delta F_x}{\Delta x} \qquad K_{yx} = -\frac{\Delta F_y}{\Delta x} \tag{15}$$

Also it is assumed here due to symmetry that the other two stiffness coefficients are given by

$$K_{xy} = -\frac{\Delta F_x}{\Delta y} = -K_{yx} \qquad K_{yy} = -\frac{\Delta F_y}{\Delta y} = K_{xx} \tag{16}$$

The impeller is displaced in the positive x-direction and the rotation is positive in the counterclockwise direction. A positive force F_x aggravates x displacements whereas a negative force resists x displacements. Thus, positive principal stiffness K_{xx}, which indicates a restoring force, is desirable. The cross-coupled force should oppose motion (for a shaft forward whirl mode) to promote rotor stability. Thus F_y should be negative and the cross-coupled stiffness K_{yx} should be positive for stabilizing effects in forward whirl.

Generally it is desired to use the calculations discussed here for rotor dynamics analysis. The stiffness is more useful than the force so stiffnesses are presented in the results section. Dimensionless stiffnesses have the form

$$\overline{K}_{ij} = \frac{K_{ij} R_3}{\frac{1}{2}\rho A_3 U_3}$$

in the next section.

RESULTS

Twelve different cases typical of pump impeller geometries were run. Table 1 gives the geometric properties. Quantities varied were number of blades, blade angle, radius ratios, and blade thickness. In each case, the following rotor parameters were held constant

ω = 600 rpm
b = 0.5 inches
ρ = 0.0361 lbm/in^3

A finite element mesh was generated for each case.

Once velocities were determined at all of the finite element node points, Eq. (14) was used to evaluate the forces acting on the impeller control volume. It should be noted that these forces calculated for the centered impeller were not zero due to the numerical averaging. However, the change in force calculated for the eccentric impeller is two to four orders of magnitude larger than the centered force. The five components of force for each case are not given here due to lack of space. They are presented in ref. (12).

The analysis described in Section 2 was carried out for the twelve cases. Table 2 presents the calculated values of dimensionless blade stream function for each blade. Here the stream function is made dimensionless via

$$\bar{\psi} = \frac{\psi}{R_3 U_3}$$

It can be seen that an eccentricity of the order of 0.001 produces changes in the blade stream function of the order of 0.001 as well.

A comparison between the theory and two experimental results can be presented. Case 4 is chosen as the closest to the test impellers of Uchida (8) and Kanki (9). Uchida employed a single volute while Kanki used a double volute. The dimensionless forces are

F_{radial}	
0.00187	Uchida, et. al. (8)
0.00122	Kanki, et. al. (9)
0.001023	Theory, Case 4

The agreement with Kanki's results is within 20%.

Table 3 gives the dimensionless principal and cross-coupled stiffnesses as determined by the finite element analysis. In all cases, the principal stiffness is negative while the cross-coupled stiffness is positive. Several patterns emerge from the series of cases run.

Cases 1 and 7-11 indicate the effect of varying blade angle β. Figure 3 indicates the stiffness variation with blade angle. The magnitude of the principal stiffness decreases strongly with increasing blade angle. However, the magnitude of the cross-coupled stiffness does not seem to be a strong function of blade angle.

The effect of number of blades can be seen in cases 1, 4, 5. Figure 4 plots the results. The magnitude of the principal coefficient increases somewhat with number of blades but, again, the magnitude of the cross-coupled stiffness does not seem to be a strong function of the number of blades.

Cases 1 and 12 indicated the effect of impeller inner to outer radius (R_3/R_2). This produced the largest change in the cross coupling stiffness. The values are

Case	R_3/R_2	$\bar{K}_{xx}$	$\bar{K}_{yx}$
1	2.0	- 0.3529	0.6057
12	3.0	- 0.1047	0.0728

Also, the effect of the other radius ratios R_1/R_2 and R_4/R_2 can be seen from cases 2,5 and 5,3 respectively. Blade thickness (cases 1,6) did not have a strong effect.

The calculated dimensionless stiffnesses can be compared to the measured values by Chamieh et. al. (10). The results are (using the sign convention for stiffness normal to rotor dynamics as defined in Section 3)

$\bar{K}_{xx}$	$\bar{K}_{yx}$	
- 2.0	- 0.9	Chamieh et. al. (10)
- 0.2987	0.6922	Case 3

The principal terms have the same sign but differ by an order of magnitude. The cross-coupled terms have the same order of magnitude but different sign.

CONCLUSIONS

This study investigates the effect of non-uniform inlet flow in two dimensional eccentric unbounded impellers. A comparison of the calculated radial force to available experimental results indicates reasonably good agreement. It seems safe to conclude that non-uniform inlet flow is an important factor in hydraulic force calculations with applications to rotor dynamics.

Comparisons of the theoretical stiffnesses to measured values are less good. Perhaps this indicates that other effects not modeled here are equally important. These are likely to include three dimensional effects, viscous effects, and volute (or diffuser) effects.

REFERENCES

1. Ek, M. C.: Solution of the Subsynchronous Whirl Problem in the High Pressure Hydrogen Turbomachinery of the Space Shuttle Main Engine. AIAA/SAE 14th Joint Propulsion Conference, Paper 78-1002, July 1978.

2. Allaire, P. E., Lee, C. C. and Gunter, E. J.: Dynamics of Short Eccentric Plain Seals with High Axial Reynolds Number. Journal of Spacecraft and Rockets, Vol. 15, No. 10, November 1978.

3. Colding-Jorgensen, J.: Effect of Fluid Forces on Rotor Stability of Centrifugal Compressors and Pumps. Proceedings of NASA/ARO Workshop on Rotordynamic Instability Problems in High-Performance Turbomachinery, NASA CP-2133, 1980, pp. 249-265.

4. Shoji, H. and Ohashi, H.: Fluid Forces on Rotating Centrifugal Impeller with Whirling Motion. Proceedings of NASA/ARO Workshop on Rotordynamic Instability Problems in High-Performance Turbomachinery, NASA CP-2133, 1980, pp. 317-328.

5. Imaichi, K., Tsujimoto, Y., and Yoshida, Y.: An Analysis of Unsteady Torque on a Two-Dimensional Radial Impeller. ASME Winter Annual Meeting, Washington, D.C., November 1981.

6. Iino, T.: Potential Interaction Between a Centrifugal Impeller and a Vaned Diffuser. ASME Winter Annual Meeting, Fluid-Structure Interactions in Turbomachinery, November 1981, pp. 63-69.

7. Allaire, P. E., Branagan, L. A., and Kocur, J. A.: Aerodynamic Stiffness of an Unbounded Eccentric Whirling Centrifugal Impeller with an Infinite Number of Blades. Proceedings of NASA/ARO Workshop on Rotordynamic Instability Problems in High Performance Turbomachinery, NASA CP-2250, 1982, pp. 323-343.

8. Uchida, N., Imaichi, K., and Shirai, T.: Radial Force on the Impeller of a Centrifugal Pump. Bulletin of the JSME, Vol. 14, No. 76, 1971, pp. 1106-1117.

9. Kanki, H., Kawata, Y., and Kawatani, T.: Experimental Research on the Hydraulic Excitation Force on the Pump Shaft. ASME paper no. B1-DET-71.

10. Chamieh, D. S., Acosta, A. J., Brennen, C. E., Caughey, T. K., and Franz, R.: Experimental Measurements of Hydrodynamic Stiffness Matrices for a Centrifugal Pump Impeller. Proceedings of NASA/ARO Workshop on Rotordynamic Instability Problems in High-Performance Turbomachinery, NASA CP-2250, 1982, pp. 382-398.

11. Busemann, A.: The Delivery Head Ratio for Radial Centrifugal Pumps with Logarithmic Blades. Zeitschrift fur Angewandte Mathematik und Mechanik, Vol. 8, No. 5, 1928, pp. 372-384.

12. Sato, C. J.: Aerodynamic Forces On An Unbounded Centrifugal Impeller Undergoing Synchronous Whirl. M.S. Thesis, University of Virginia, August 1982.

13. Stanitz, J.: Personal Communication, 1981.

14. Zienkiewicz, O. C.: The Finite Element Method. McGraw-Hill Book Company, New York, 1977, pp. 677-757.

15. Bathe, K. and Wilson, E. L.: Numerical Methods in Finite Element Analysis. Prentice-Hall, Inc., New Jersey, 1976, pp. 203-213.

16. Fox, R. W. and McDonald, A. T.: Introduction to Fluid Mechanics, John Wiley & Sons, New York, 1978, p. 166.

TABLE 1 - IMPELLER GEOMETRIES FOR TWELVE CASES

Case No.	No. of Blades	Blade Angle	R_1/R_2	R_4/R_2	Thickness (inches)	R_3/R_2	θ_s
1	4	30	0.5	2.5	1/8	2.0	-140
2	3	30	0.25	2.5	1/8	2.0	-140
3	3	30	0.5	2.75	1/8	2.0	-140
4	7	30	0.5	2.5	1/8	2.0	-140
5	3	30	0.5	2.5	1/8	2.0	-140
6	4	30	0.5	2.5	3/16	2.0	-140
7	4	16	0.5	2.5	1/8	2.5	-152
8	4	22	0.5	2.5	1/8	2.5	-143
9	4	26	0.5	2.5	1/8	2.5	-140
10	4	37	0.5	2.5	1/8	2.5	-107
11	4	45	0.5	2.5	1/8	2.5	- 95
12	4	30	0.5	2.5	1/8	2.5	-178

TABLE 2. DIMENSIONLESS VALUES OF BLADE STREAM FUNCTION FOR IMPELLER SHAPES

Case	No. of Blades		Centered Impeller	Blade Stream Functions: Eccentric Impeller (ε/R_2 = 0.0025) (1)	(2)	(3)	(4)	(5)	(6)	(7)
1	4	30	.2062	.2056	.2058	.2068	.2065			
2	3	30	.1941	.1934	.1942	.1949				
3	3	30	.1505	.1499	.1507	.1511				
4	7	30	.2440	.2435	.2434	.2437	.2442	.2445	.2444	.2439
5	3	30	.1941	.1933	.1941	.1948				
6	4	30	.2123	.2117	.2120	.2129	.2126			
7	4	16	.3115	.3112	.3114	.3118	.3116			
8	4	22	.2697	.2693	.2695	.2701	.2700			
9	4	26	.2365	.2360	.2362	.2370	.2368			
10	4	37	.2276	.2275	.2268	.2277	.2284			
11	4	45	.2253	.2254	.2244	.2252	.2262			
12	4	30	.1588	.1586	.1588	.1590	.1588			

TABLE 3. PRINCIPAL AND CROSS COUPLED STIFFNESS OF TWELVE IMPELLER CASES

Case Number	Principal Stiffness K_{xx}	Cross Coupled Stiffness K_{yx}
1	-0.3529	0.6057
2	-0.2145	0.6523
3	-0.2052	0.5197
4	-0.5571	0.6025
5	-0.2988	0.6922
6	-0.4446	0.6055
7	-0.8532	0.2525
8	-0.5807	0.4345
9	-0.3968	0.5011
10	-0.1423	0.4506
11	-0.1203	0.3940
12	-0.1047	0.0728

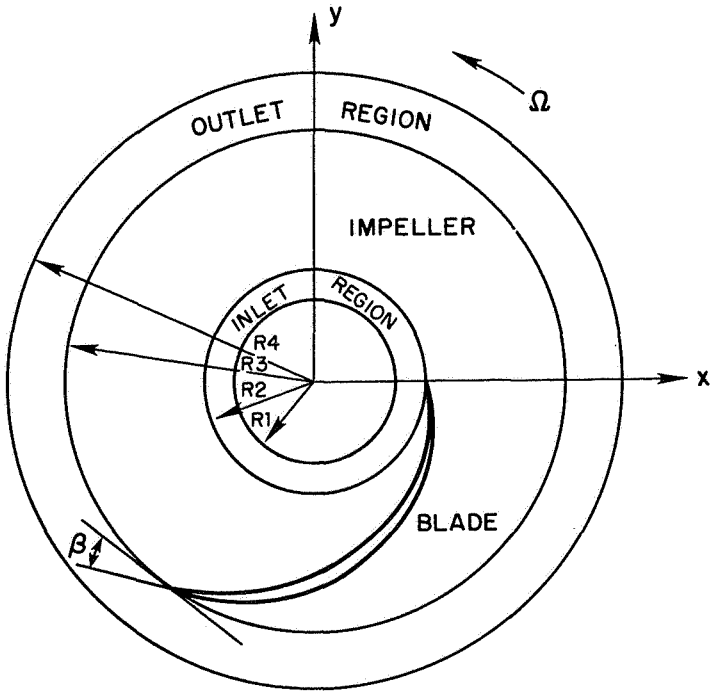

Figure 1. Impeller Geometry

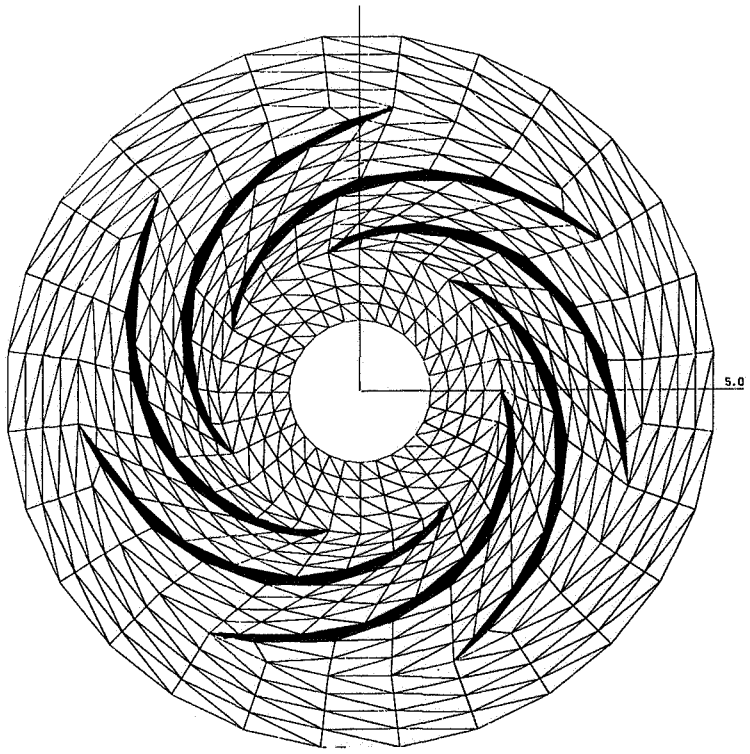

Figure 2. Finite Element Model for Case 4 - Seven Bladed Impeller (560 Nodes and 952 Elements)

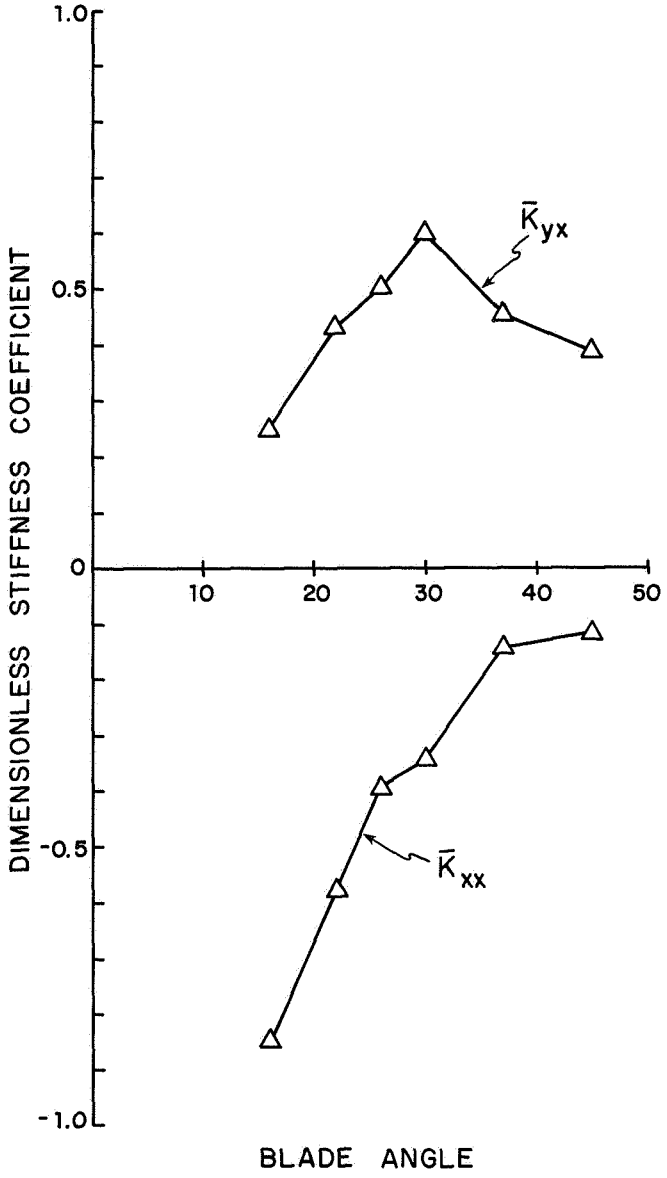

Figure 3. Stiffness vs. Blade Angle (Cases 1 and 7-11)

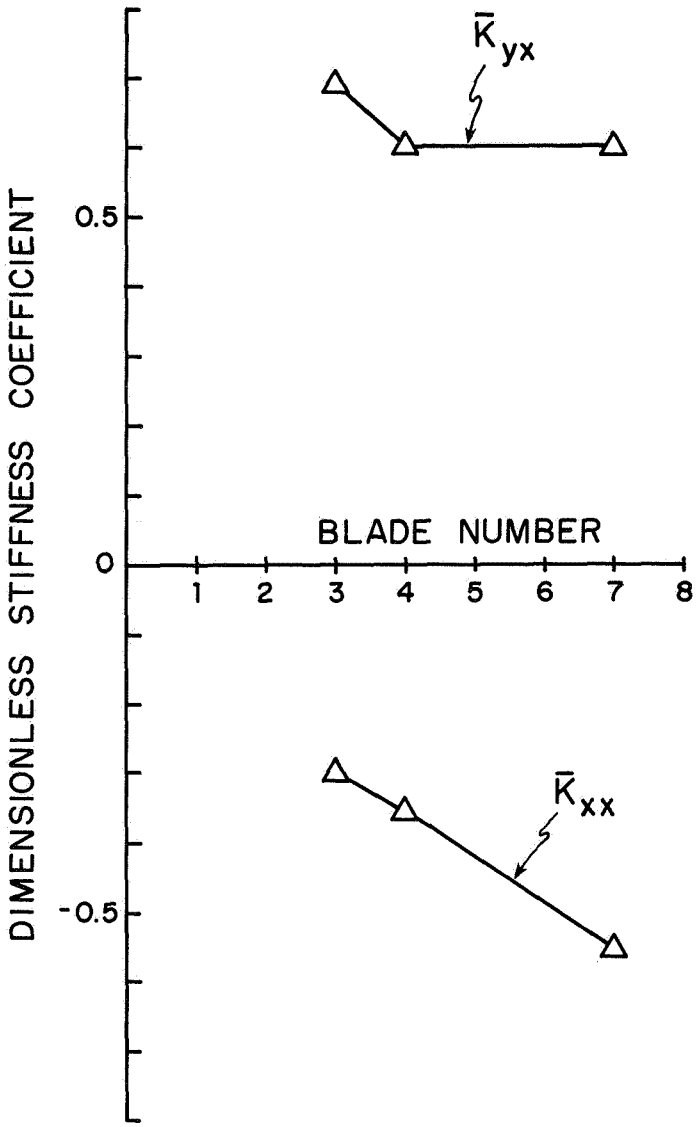

Figure 4. Stiffness vs. Blade Number (Cases 1, 4, 5)